A 1 mm-Thick Miniatured Mobile Soft Robot With Mechanosensation and Multimodal Locomotion

Zemin Liu, Jiaqi Liu, He Wang, Xiao Yu, Kang Yang, Wenbo Liu, Shilin Nie, Wenguang Sun, Zhexin Xie, Bohan Chen, Shuzhang Liang, Yingchun Guan, and Li Wen

***Abstract*—The miniature soft robots have many promising applications, including micro-manipulations, endoscopy, and microsurgery, etc. Nevertheless, it remains challenging to fabricate a miniatured robot device that is thin, flexible, and can perform multimodal locomotor mobility with sensory capacity. In this study, we propose a miniatured, multi-layer (two shape memory polymer layers, a flexible copper heater, a silk particle enhanced actuator layer, and a sensory layer) four-limb soft robot (0.45-gram, 35 mm-long, 12 mm-wide) with a total thickness of 1 mm. A precise flip-assembling technique is utilized to integrate multiple functional layers (fabricated by soft lithography, laser micromachining technologies). The actuator layer's elastic modulus increased ∼100% by mixing with 20% silk particles by weight, which enhanced the mechanical properties of the miniature soft robot. We demonstrate that the soft robot can perform underwater crawling and jumping-gliding locomotion. The sensing data depicts the robot's multiple bending configurations after the sensory data been processed by the microprocessor mounted on the robot torso. The miniatured soft robot can also be reshaped to a soft miniatured gripper. The proposed miniatured soft robots can be helpful for studying soft organisms' body locomotion as well as medical applications in the future.**

***Index Terms*—Soft robot materials and design, soft sensors and actuators.**

Manuscript received September 7, 2019; accepted January 20, 2020. Date of publication February 26, 2020; date of current version March 9, 2020. This Letter was recommended for publication by Associate Editor R. Niiyama and Editor K.-J. Cho upon evaluation of the reviewers' comments. This work was supported in part by the National Science Foundation support projects, China under Grant 61633004, in part by National Key R&D Program of China under Grant 18YFB1304600, and in part by National Science Foundation support projects under Grants 61822303, 91848105. *(Corresponding author: Li Wen.)*

Zemin Liu, Jiaqi Liu, He Wang, Wenbo Liu, Shilin Nie, Wenguang Sun, Zhexin Xie, Bohan Chen, Shuzhang Liang, and Yingchun Guan are with the School of Mechanical Engineering and Automation, Beihang University, Beijing 100191, China (e-mail: zeminliu@buaa.edu.cn; jiaqiliu@buaa.edu.cn; wanghe1314@buaa.edu.cn; wenboliu@buaa.edu.cn; nieshilin@buaa.edu.cn; buaaswg@126.com; zhexinxie@buaa.edu.cn; albertchen@buaa.edu.cn; liangsz13nq@buaa.edu.cn; guanyingchun@buaa.edu.cn).

Xiao Yu is with the Department of Mechanical Engineering, Johns Hopkins University, Baltimore, MD 21218-2683 USA (e-mail: xyu52@jhu.edu).

Kang Yang is with the International Research Center for Advanced Structural and Biomaterials School of Materials Science and Engineering, Beihang University, Beijing 100191, China, and also with the School of Mechanical Engineering and Automation, Beihang University, Beijing 100191, China (e-mail: qingyang1122@126.com).

Li Wen is with the School of Mechanical Engineering and Automation, Beihang University, Beijing 100191, China, and also with the Beijing Advanced Innovation Center for Biomedical Engineering, Beihang University, Beijing 100191, China (e-mail: liwen@buaa.edu.cn).

This letter has supplementary downloadable material available at http://ieeexplore.ieee.org.

Digital Object Identifier 10.1109/LRA.2020.2976306

I. Introduction

MINIATURED soft robots are promising because of their compact size, high mobility, and precise operability [1], [2]. These features endow soft robots with possible applications in the medical field, such as the tissue-engineered biohybrid soft robot [3], microscale objects manipulation [4], [5], and minimally invasive surgery [6], etc. Manufacturing technologies play a crucial role in the fabrication of such type of soft robot. The molding-casting method was commonly used to fabricate centimeter-scale soft robots [7]. Advancing in 3D printing technology was applied to manufacture bio-inspired soft robots with complex geometries [8]–[10]. Soft lithography and laser machining enabled the fabrication of microfluidic chambers [11], [12], as well as self-assembling microstructures for soft actuators [13]. Besides, various smart material actuated micro soft robots have been developed, such as hydrogel micropatterning [14], and materials responsive to electricity [15], light [16], temperature [17], and magnetic field controlled small scale soft robots have been developed for drug delivery [18], surgery [19] and generating aquatic biomimetic swimming [2]. Besides, soft devices, including soft computer [20] and soft pump [21] may also shed light on the entire soft miniatured robots.

Recently, emerging attentions were paid to create sub-millimeter, flexible, miniatured robotics which may endow future medical robotic applications [6]. Besides possible application in medical [3], [6] and flexible electronics [11], the creation of thin, flexible soft robots with locomotion capacity may also shed insights into the biomechanics study of soft-bodied marine animals that has membrane-like body or fins, such as the rays, jellyfish, sea eel (Leptocephalus).

Although the previous fabrication techniques and new materials have emerged, however, it remains challenging to fabricate a miniatured robot device that is thin, flexible, and can perform multimodal locomotor mobility with sensory capacity. Actuator design and material choices play an essential role in generating multimodal locomotion of the soft robot [22]. Incorporating sensory system to the miniatured soft robots is another technological challenge. In this study, we aim to address the following issues: 1) How to integrate multi-functional materials in a miniatured soft robot which allows multimodal locomotion? 2) How to implement mechanosensation and onboard data processing on the robot?

By utilizing a flip-assembling mechanism, multiple functional layers (fabricated by soft lithography and laser micromachining)

are bonding together after surface modification via plasma. The thickness of each layer is no more than 200 μm, after bonding all five layers precisely, resulting in a soft robot with a total thickness of 1 mm. Microscale silk particles were applied to the actuator layer to enhance its mechanical properties. The SMP layer is used to tuning the stiffness according to the thermal control of the laser cut heater. Pneumatically actuating the microfluidic chambers by time sequence allows the robot to perform crawling and jumping-gliding motion underwater. Meanwhile, the robot's four limbs' bending configuration can be identified by the micro-fabricated liquid metal (EGain) layer [23], which functions as the electronic sensory skin [24], [25]. A microprocessor is incorporated to process the sensing data then feed the data back to pneumatic system's controller. The robot can also be manually reshaped into a four-fingered gripper for pick-place small items.

II. Materials and Methods

The potential application of the miniatured quadruped soft robot is shown in Fig. 1(a). The micro soft robot is composed of 5 functional layers Fig. 2(f), the sensory layer: the actuator layer (reinforced by silk particles), two SMP layers, and the heating layer. The thickness of each layer is no more than 200 μm. A microprocessor was employed to filter the sensory data. The basic principle of the actuation is that the air pressure inflates the upper layers (actuator layer and sensory layer) and then generate the bending motion given that the SMP layer at the bottom is not stretchable.

To fabricate the heater layer, a flexible thin (5μm in thickness) constantan foil was cut by a high-resolution picosecond laser beam (600 PS pulses at 200 kHz repetition rate, 1064 nm in central wavelength) (Fig. 2(a)). The laser beam was produced by the precisely controlled laser system (PicoYL-15-0.1, Anyang Laser Technology Co., Ltd., China). The constantan foil has high electrical resistivity ($5.0 \times 10 - 7\ \Omega$·m), which enables the heater high electro-heat conversion capacity. After laser cutting, we soldered silver wires to the pins of the heater.

The SMP layer was fabricated by the SMP epoxy (EPON 828, Hexion Inc., USA) and Jeffamine D400 (Huntsman Polyurethanes Ltd, China) with a ratio of 10:6 by weight. We poured this mixture material on top of a silicon wafer and degassed in the vacuum chamber at -100 kPa for 5 min. Then, the wafer was rotated at 200 rpm for the 80 s to create layers with a thickness of $\sim$200 μm. The laser-cut thin heaters were then patterned in the uncured SMP layer. The liquid state SMP compound would be encapsulated around the heaters, which will enable the circuit's thermal energy to transmit rapidly through such a thin film to speed up the phase transition. The SMP compound embedded with heaters was finally cured after a series of the heating process: first heated in an oven at 60 °C for three hours, and then heated at 80 °C for one hour, and finally heated at 100 °C for half an hour, then it is ready.

The actuator layer was reinforced by silk particles (more details will be discussed in Section III). SU-8 2050 photoresist (MicroChem Corp.) was utilized to fabricate the micropatterns (height of the features is 100 μm) on blank silicon wafers via

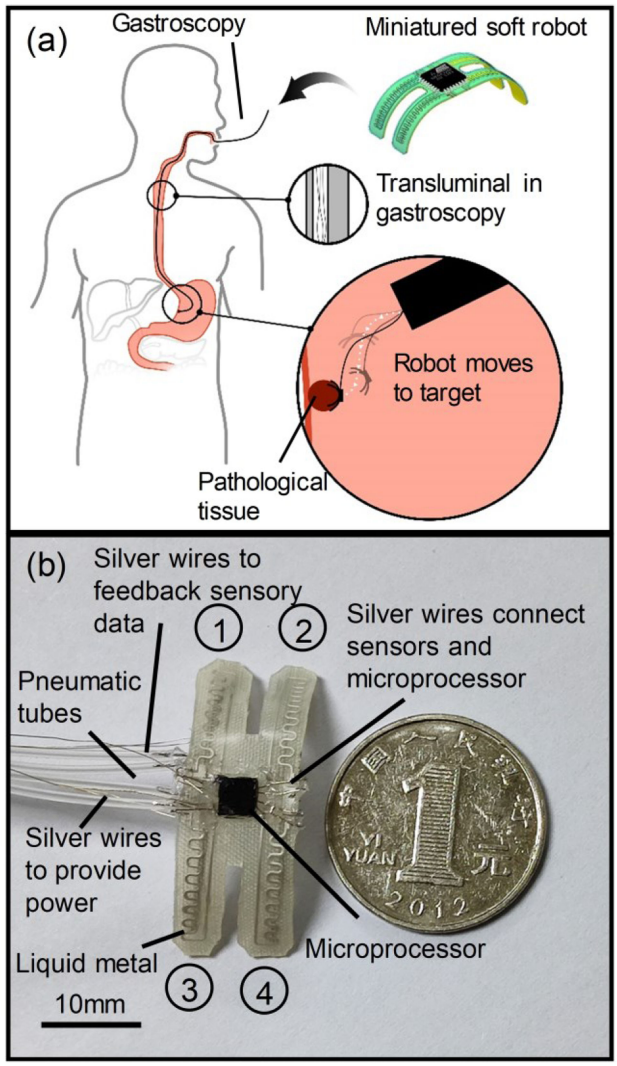

Fig. 1. Overview of the design. (a) Blueprint of the miniatured thin soft robot in a gastroscopy-based surgery. Potentially, the miniatured soft robot can be delivered into human stomach via a gastroscopy. The pneumatic tubes and wires can be transmitted through the transluminal inside the gastroscopy. With the help of gastroscopy, the mobile soft robot may function as 'surgical end effector' to remove pathological tissue in the future. (b) A snapshot of this miniatured soft robot. Inflating compressed air into microfluidic chambers via tubes enables the robot to move with four limbs which were numbered in the figure. The upper sensing layer can perceive the limbs' bending configuration. The microprocessor was used to acquire and process the sensory data of bending. The sensory data was feedback to a control board with microprocessor via silver wires. Scale bar: 10 mm.

the soft lithography technology. Wafers with micro-patterns were placed in an evacuated chamber containing a few drops of trichloro (1H, 1H, 2H, 2H-perfluorooctyl) silane (Sigma Aldrich) for 4 h, then baked in an oven at 90 °C for 45 min. Sylgard 184 (Dow Corning) were mixed at a ratio of 10:1 (base: curing agent) and degassed in a vacuum chamber for 5 minutes, then poured onto prepared blank wafers. After spin coating at 420 rpm for 80 s, an actuator layer with a thickness of 200 μm can be obtained. The sensing layer was fabricated by using the same method as the actuator layer. Ecoflex 20 was chosen for the sensing layer because it has low young's modulus and can

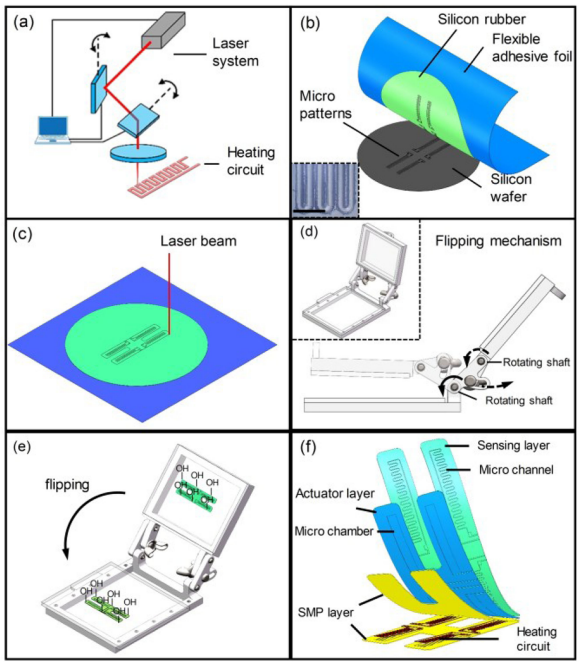

Fig. 2. The fabrication process of component layers with microstructures and the mechanisms for the flip-assembling technique. (a) The fabrication process of the heating layer. A precisely controlled laser system is utilized to cut the thin constantan foil (5μm in thickness) to fabricate the heater. (b) Peeling the sensory layer spin-coated and cured on a SU-8 patterned wafer using a flexible and adhesive foil. The inset panel indicates the image of the SU-8 micro patterns under an optical microscope (scale bar: 200 μm). (c) Laser cutting the sensory layers to form the quadruped robot's shape. The pneumatic actuator layer was fabricated by the methods shown in (b) and (c). (d) The CAD model of a flipping mechanism for bonding adjacent layers. The rotating shafts can adjust the position of the two plates (misalignment error is around 40 μm). (e) The assembling process of the sensing layer and the other part. Oxygen plasma was employed for surface modification. The surface of the layer formed chemical bonds after been treated by plasma. Soft layers can be bonded via this approach within 60 seconds. The assembled part and the sensing layer were placed on the plates for precise positioning. (f) Five layers composing the soft robot. Two stiffness-tunable layers (SMP layers), a heating circuit layer, an actuator layer, and an EGain sensor layer are shown in an exploded view.

minimize the sensory layer's influence on the bending motion. Ecoflex 20 were mixed at the standard 1:1 ratio, degassed and spin-coated at 300 rpm for 90 s. After cured under 30 °C for 1 h, we obtained a 200 μm thick sensing layer.

The sensory layer and actuator layer were peeled off from the patterned silicon wafers by flexible yet inextensible substrates (Gel-Pak 8 film, Gel-Pak©) (Fig. 2(b)). The substrates could protect the soft layers from being polluted by dust.

All function layers were completed. Subsequently, these layers were cut using a preciously controlled laser system according to the designed quadruped shape (Fig. 2(c)). The cutting misalignment error is about 40 μm.

We developed a flip-assembling mechanism for the subsequent precise bonding of functional layers. The distance between the two plates is tunable by rotating the plates around the shaft (Fig. 2(d)). Adjacent layers were placed on the mechanism's plates; then, a pre-flipping motion would be conducted to check the position of the layers. After the inspection, the mechanism with functional layers would be placed in a chamber for surface modification (oxygen plasma). The surface of the layer formed chemical bonds after being treated by plasma. Different soft silicone layers could be bonded together via the plasm method within 60 s. Flipping the plates slowly (avoid bubbles, the operating time is no more than 60 s) then the adjacent layers would be precisely bonded. The misalignment error during the flipping-bonding process has been reduced to 40 μm due to the operation under a microscope. After flipping all layers into place via this device, we gently pressed the layers on top for better bonding using a tweezer. During pressing, we carefully avoided pressing areas on top of the micro-channels to prevent deforming the micro-channels. Fig. 2(e) illustrates the bonding process of adjacent layers. In this way, we manufactured multilayer laminate millimeter-scale soft robot with embedded features. We also transformed the 2-dimensional features (one soft layer) into a three-dimensional soft robot (the multilayer quadruped soft robot) using this fabrication method. Afterwards, the liquid metal (EGain) was injected into the sensor microchannels to function as a soft sensor. Silver wires were inserted in the sensor microchannels and then soldered to the microprocessor (Fig. 1(b)) (mounted on the robot torso by silicon rubber) for transmitting the sensory data. And additional silver wires would connect the microprocessor to an Arduino board (MEGA328P), which functioned as the pneumatic system controller. Finally, flexible tubes (with internal diameter of 200μm) was inserted into the actuator microchannels. To minimize the influence of tubes and wires on the robot's locomotion, all the tubes and wires were connected to the side of the soft robot. Through multiple trials, we found that this side-connected way reduced the effect of the flexible tubes and wires on the robot's locomotion.

The flipping mechanism is necessary for the following reasons: 1) With the samples' pre-positioning on the plates, the mechanism can achieve precise bonding (positioning accuracy is critical in the fabrication process of millimeter-scale robots). 2) After surface modification, there is only one chance and 60 s left for the bonding process. With the help of the flipping mechanism, the bonding process can be done precisely within 10 s.

It is difficult to find an appropriate customized air valve to actuate the robot as the required inflated air volume is quite small due to the size of the micro-chambers. Therefore, we designed a syringe-pneumatic system (Fig. 3) to actuate this miniatured soft robot. Controlled by the PWM signals by an Arduino board, the servo motor could drive the link mechanism to push the syringes to change the volume of the air, thus to generate tunable air pressure. The air pressure was calibrated by a SMC barometer (PSE300-MLA). This syringe-induced compressed air was injected to the actuator chambers via the flexible tubes. Details are also provided in the supplementary video. Meanwhile, the microprocessor on the robot acquired and filtered the sensory data, which was sent to the Arduino control board to feedback the limbs' bending.

III. Results

A. Mechanical Properties of the Actuator Layer

The actuator layer is the most essential functional layers of the miniaturized, thin soft robot. Existing research shows that fibers

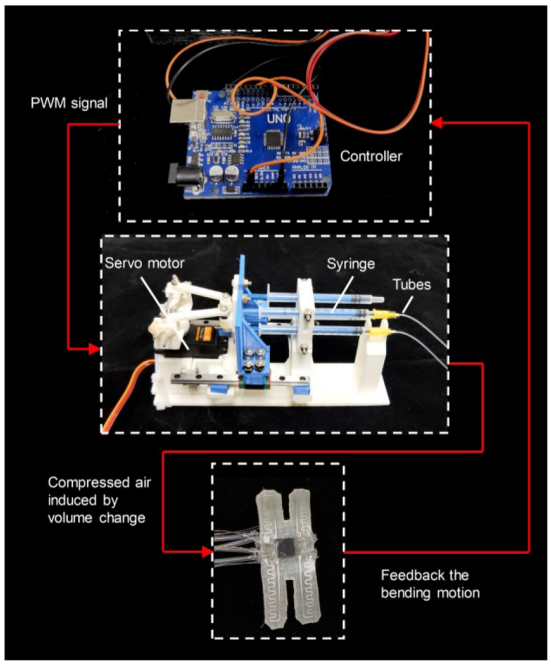

Fig. 3. The pneumatic actuation and control system for the soft robot. The actuation system consists of one servo motor, a linkage mechanism, and several syringes (two of them are used). The total volume of each syringe is 1 mL. The sensory data can feedback limbs bending motion to the controller which also generate PWM signal for the servo motor.

reinforce the soft robots in terms of force output and ballooning effect constraining [26], [27]. In current study, we applied silk particles and fibers to reinforce the actuator layer's mechanical properties. 6 kinds of actuator layers with different components (Fig. 4(d)-Fig. 4(i)) were tested their mechanical properties via the universal tensile test machine (Tensilon HZ-1004D, Hengzhun Instrument Technology Co., China). The machine was programmed to stretch the sample (sample's size: 20 mm $\times$ 10 mm, 200 μm in thickness) at 10 mm/min.

Samples' tensile strength significantly increased as more silk particles were mixed in the Sylgard 184, yet more silk particles also induced lower tensile fracture limit (Fig. 4(b)). A large tensile strength can sustain large air pressure thus to generate considerable force during the locomotion, while low tensile fracture limit would result in an easy fracture. Therefore, there is a trade-off between the tensile strength and tensile fracture. When the silk fibers (50 μm in thickness) and flax fibers (60 μm in thickness) were embedded in the PDMS (Sylgard 184), there was a significant increase in the tensile strength compared with the pure PDMS and samples mixed with silk particles. However, the fibers are not stretchable. The actuator layer should be stretchable with relatively high tensile strength and high fracture limit. Taking all the factors into consideration, we decided to choose the PDMS mixed with 20% silk particles for the actuator layer.

B. Mechanical Thermal Properties of the SMP Layer

Dynamic mechanical thermal analysis (DMTA) was employed to test the SMP layer's mechanical properties as a function of temperature, frequency and time. The SMP layer's thermo-mechanical properties could be precisely obtained by this experiment. Thermomechanical experiments were conducted on thin shape memory polymer samples. Samples' size is 3.5 mm x 10 mm x 200 μm. A dynamic mechanical thermal analyzer (DMA Q800, TA instrument Technology Co., USA) was utilized to determine the temperature influence on the transition regime's modulus. The SMP samples were cycled at a frequency of 1 Hz between the maximum and minimum stretching stress, the maximum stretching strain was 0.2%. The temperature was programed to increase from -30 °C to 90 °C, at the step of 3 °C per minute. As defined by the tan delta peak, the glass transition temperature is approximately 57 °C (Fig. 5(a)). Around the glass transition temperature, the SMP layer's modulus decreased significantly. At 25 °C, the material's elastic modulus is about 1905 MPa. When the SMP layer was heated to 30 °C, its elastic modulus decreased significantly. After heated to the glass transition temperature (57 °C), the value reduced to 12 MPa. Transferred from rigid state to the soft state, the elastic modulus decreased about 160 times. Noted that, the SMP layer is very thin (200 μm in thickness) and the temperature difference between the two states is about 30 °C, which requires less time to achieve the phase transition via the efficient heating circuit.

To evaluate the SMP layer's phase transition time as a function of the heater's power, an infrared camera (Ti400, Fluke Thermography, USA) was employed to record the layer's temperature change at a frame rate of 9 Hz. We applied different direct current to the heater to produce different heating power. Then the infrared videos were processed with the software (SmartView 4.1, Fluke Thermography, USA) to get the temperatures by time series. As Fig. 5(b) shows, the SMP layer's phase transition time decreases as the heater's power increases. Notably, when the heating power reaches 1 W, the phase transition time could be reduced to about 1 s. The inserted infrared images (Fig. 5(b)) shows the prototype's heating process in time series. Noted that, the cooling process took about 1 min in the air for the robot cooled under phase transition temperature, and this process was within 10 s when the prototype worked underwater. The heating time took about 15 s (with an input power of 1 W) for the robot to be softened when the robot was just emerged underwater. It was difficult to record the temperature once the robot was entirely emerged underwater.

C. The Sensory Capacity of the Sensing Layer

Soft sensor's (sensor 1) relationship between inflated air pressure and ΔR/R is depicted in Fig. 6(a). ΔR/R increases with increased inflating pressure. Meanwhile, we also tested the relationship between the limb's (limb 1) curvature and air pressure (Fig. 6(b)). Consequently, the actuator layer's bending configurations could be identified by the soft sensor's output, which will play an important role in the closed-loop control. The compressed air was generated by the syringe-pneumatic system and air pressure was calibrated by a SMC barometer.

Fig. 7 shows the soft sensor's dynamic response. The sensor has slight hysteresis when the actuator layer was inflated under

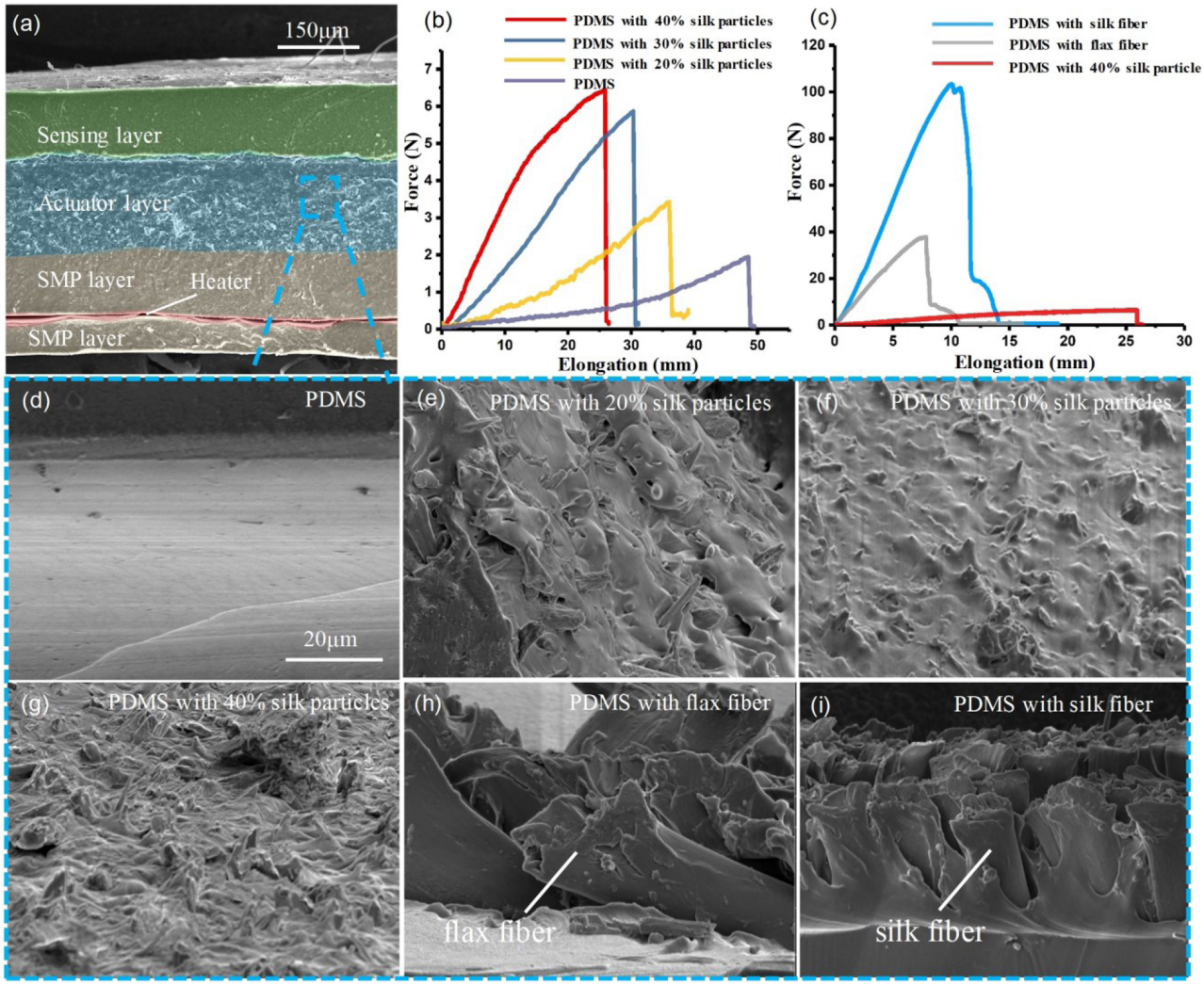

Fig. 4. Actuator layer with microscale silk composite (200 μm in thickness). (a) The ESEM image illustrates the robot's layered structure, scale bar: 150 μm. (b) The elongation-force relationships of the pure PDMS sample and samples of PDMS mixed with silk particles by different weight rate. Sample size is 20 mm $\times$ 10 mm, and the thickness is 200 μm. (c) The elongation-force relationships of the PDMS mixed with 40% silk particles, PDMS embedded with flax fiber, and silk fiber. (d)-(i) illustrate the actuator layer with different materials. (d) ESEM image of pure PDMS. (e) ESEM image of PDMS mixed with 20% (by weight) silk particles. (f) ESEM image of PDMS mixed with 30% (by weight) silk particles. (g) ESEM image of PDMS mixed with 40% (by weight) silk particles. (h) ESEM image of PDMS embedded with flax fiber. (i) ESEM image of PDMS embedded with silk fiber. The scale bar of (d)-(i) is 20 μm.

square wave function, which is shown in Fig. 7(a). A possible explanation for this might be that the inflating air compressed the microchannels, so it took time for the elastomer materials to recover the shape (elastomer materials' viscoelasticity). The soft sensor performed great repeatability under the sine wave inflation-deflation cycle (Fig. 7(b)). As the robot would work at a temperature of around 57 °C, we measured the resistance of the soft sensor from 25 °C to 60 °C. We found that the resistance changed $\sim$2.5% within this temperature range. As a result, we consider that this is acceptable while the robot performs the bending motion.

D. Multi-Locomotion and Sensory Feedback Analysis

Inspired by the cephalopod's propulsion [28], we programed a jumping-gliding motion to demonstrate the robot's capacities (supplementary video). In nature, soft-bodied earthworm use crawling locomotion to feed [29]. The miniatured soft robot can also perform crawling motions (see supplementary video). During all the motions, the SMP layer was heated to the softened state. All locomotion modes of the robot were tested underwater.

During the bio-inspired jumping-gliding motion, the microprocessor filtered the soft sensors' data, then feedback the data to the pneumatic system control board. Four limbs of the robot were inflated simultaneously (through the syringe-pneumatic system) to enable the robot leaping upward. The miniatured soft robot was actuated by two syringes, the upper syringe actuated the two anterior limbs through a one-to-two interface, while the lower syringe actuated the two posterior limbs, a servo motor pushed these two syringes through a linkage mechanism (see supplementary video). To generate the horizontal movement, a tiny phase difference (about 10°) was applied between the anterior limbs and posterior limbs during the inflating procedure (Fig. 8(c) $t = 0$ s–Fig. 8(c) $t = 0.28$ s). First, the anterior actuators

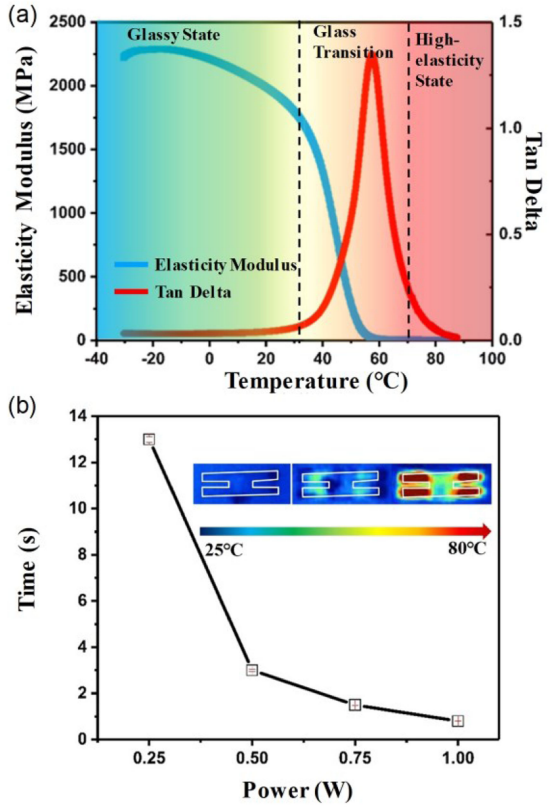

Fig. 5. Mechanical properties of the SMP layer. (a) Modulus of the SMP layer as a function of temperature. As defined by the tan delta (as a ratio of loss modulus over the storage modulus) peak, the glass transition temperature is approximately 57 °C. (b) The SMP layer's phase transition time as a function of the input power. Inset panel was the infrared image which illustrated the four limbs' heating process. The white line indicates the profile of the soft robot.

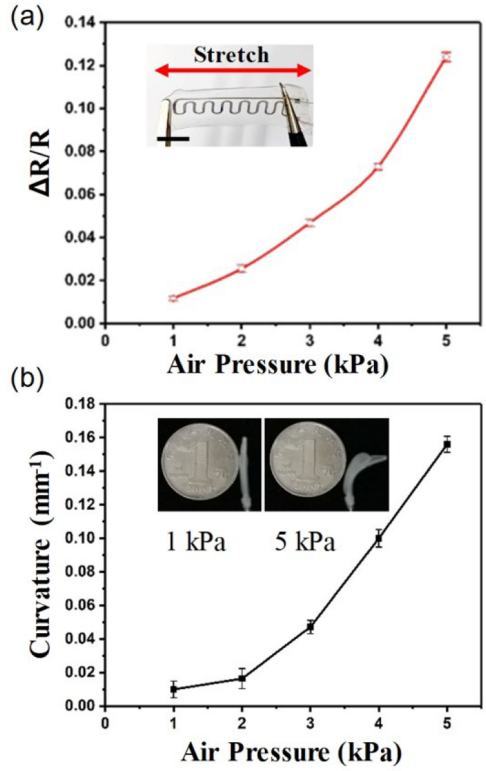

Fig. 6. Calibration results. (a) The resistance variation as a function of air pressure. Insert panel was the snapshots of one ultra-thin soft sensor, scale bar: 5 mm. (b) The single limb curvature calibration results as a function of air pressure. Insert panel was the snapshots of one limb under different air pressure.

were inflated (Fig. 8(c) $t = 0.11$ s); the robot, therefore, has a tendency to move forward. Then, the posterior actuators were inflated and bent to their maximum curvature (Fig. 8(c) $t = 0.28$ s); this operation induced the robot leaping off the ground and moved obliquely upward. We preset the phase difference mechanically through the linkage mechanism and the syringe-pneumatic system.

After jumping and releasing, the robot entered the gliding mode ((Fig. 8(c) $t = 0.7$ s–1.25 s)). The releasing process was relatively slow, thus the residual air could provide enough buoyancy to endow the robot with a proper body altitude which is similar to a jellyfish, which contract to control the body's buoyancy [30]. Finally, the robot landed on the ground. By continuously performing this reversible jumping-gliding process, the soft robot achieved smooth underwater locomotion (supplementary video). Fig. 8(b) illustrates the robot's center of mass trajectory during the continuous jumping-gliding locomotion. Applying an inflating-deflating frequency at 1 Hz, the robot achieved a horizontal movement speed at ∼0.9 BL/s (BL means body length, body length = 35 mm) and a maximum jumping height of ∼0.8 BL. Besides, the limbs bending data was filtered by the onboard microprocessor and then feedback to the controller. Four limbs were actuated by one servo motor, in order to avoid

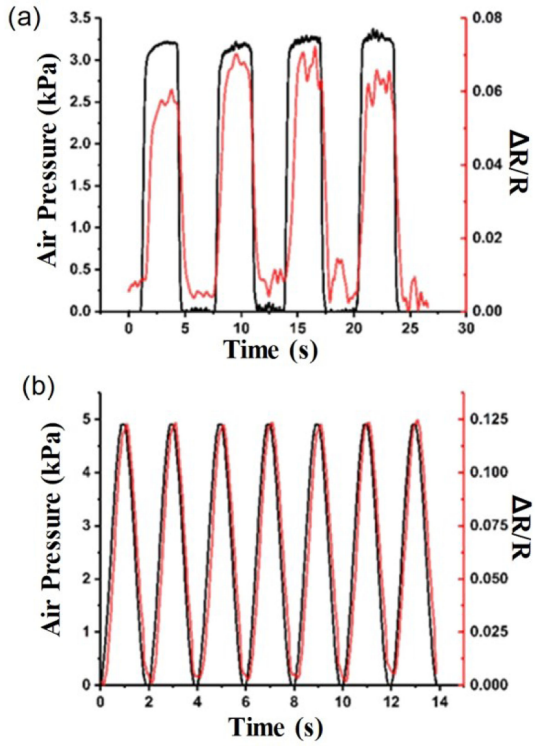

Fig. 7. Results of the sensory test. (a) The soft sensor's dynamic response when the air pressure executed a square wave function. (b) The soft sensor's dynamic response when the air pressure executed a sine wave function.

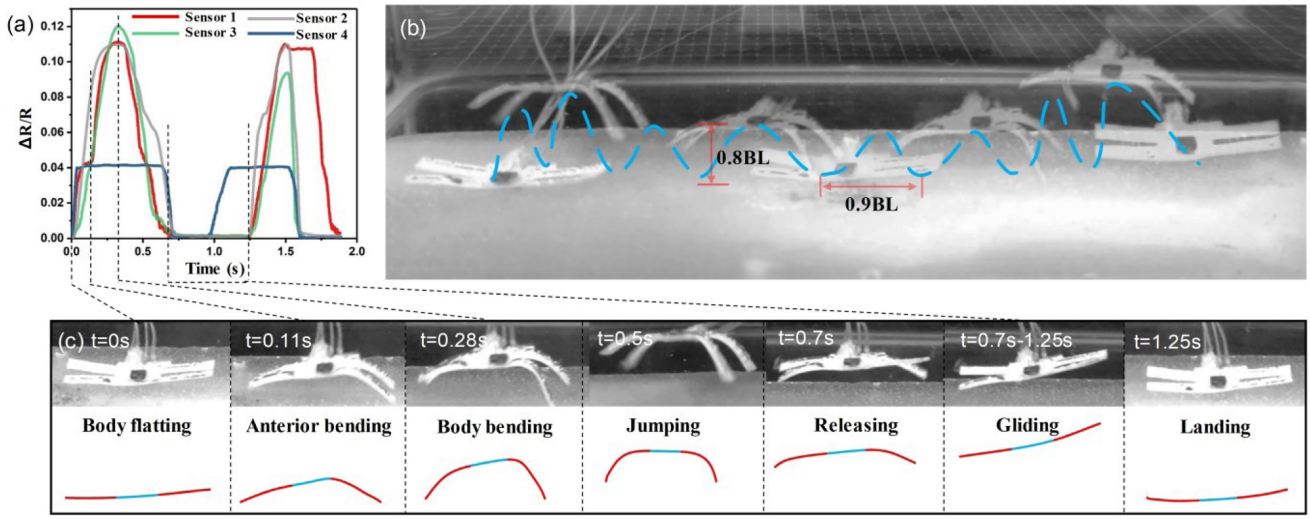

Fig. 8. Soft sensors' feedback and gaits analysis. (a) Soft sensors' feedback when the miniatured soft robot performed the jumping-gliding locomotion. (b) Quadruped soft robot in jumping-gliding locomotion. Blue dotted line was the trajectory trace. Its jumping height was 0.8 BL and gliding distance was 0.9 BL. (c) Robot's gaits in one jumping-gliding cycle. Upper panel was the snapshots in time series, the lower panel was the corresponding simplified gaits, the red curve indicates the heated section and the blue curve indicates the cooled section. The dotted line illustrates the corresponding time in (a).

actuator chambers' explosion, the maximum air pressure was limited by tuning the pushing distance of the syringe.

Fig. 8(a) depicts the soft sensors' feedback for the two moving cycles. It should be noted that in the first two cycles, limb 1–3's bending curvature were larger than that of limb 4. In addition, after being inflated to certain curvature, limb 4 maintained the shape for a short period of time, which resulting in a flat top of the sine wave, this may be induced by: 1) the microchannel deviation resulting from the fabrication process; 2) the unstable connection between the pneumatic system and the linkage mechanism.

In the two limbs crawling mode, two limbs on each side were actuated simultaneously, thus to crawl forward (supplementary video). When inflated by the syringe-pneumatic system, the left side of the robot would bend, which drove the body forward. The compressed air cycles with a frequency of 1 Hz, and the crawling speed is about 0.7 BL/s. The two limbs mode enhances the soft robot's fault tolerance - the robot can move even two limbs failed.

Besides the crawling and jumping-gliding motion, this soft robot can also function as a miniatured soft gripper. As Fig. 9(a) shows, the robot was heated to a soft state, then we manually bent the soft robot torso and reshaped the robot to a gripper. After cooled, a four-limb soft gripper was formed. Since the gripper's torso was curved, the microprocessor could not stick on a curved surface. The microprocessor was not used in this sample. During the working process, the four limbs were heated to a soft state for bending configuration (the torso was unheated). Meanwhile, the sensor's output was recorded via precision multimeter (Fluke 8845A, Fluke Inc., USA) and the data was not fed back to pneumatic system. This re-shaped soft robot can pick small object to demonstrate its capacities as a micro-gripper (supplementary video).

The maximum weight that the reshaped gripper can grasp is about 4.3 gram, almost 10 times than its own weight. The soft sensor could be used to perceive gripper's working conditions in

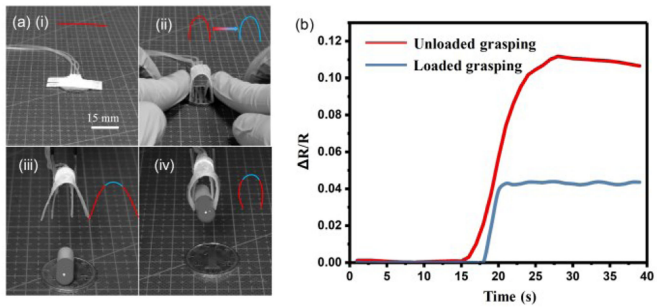

Fig. 9. Soft robot manually reshaped to a four-fingered gripper and the soft sensor's feedback during the grasping process. (a) The reshaping process (i)-(ii), the grasping process (iii)-(iv). The curve illustrates the heating section, the red curve indicates heated and blue curve indicates cooled. The scale bar of (i)-(iv) is 15 mm. (b) One soft sensor's feedback when the soft robot functioned as a micro soft gripper.

the grasping procedure. For instance, when the gripper grasped the capsule, the sensor's output value is significantly lower compared to an unloaded grasping (Fig. 9(b)) under the same air pressure. When the gripper successfully grasped, the object would prevent the fingers' further deformation, thus the output sensor value is lower than the unloaded condition. Equipped with the onboard sensory system, our miniatured soft robot has the ability to identify various bending motions.

IV. Conclusion

In summary, we developed a multi-layer, multi-function miniatured soft robot. To achieve specific function at a miniatured scale, we fabricated multiple soft functional layers with various materials. Totally five functional layers (200 μm thick for each layer) were assembled to a thin, soft robot (1 mm in thickness) via a flip-assembling mechanism. After cut by the laser system, all the functional layers were bonded evenly via

the flipping mechanism and oxygen plasma. To enhance the miniatured soft robot's mechanical properties, we mixed 20% silk particles, the actuator layer's elastic modulus increased over 100%, which endows a thin actuator layer (200 μm) with the enhanced force for bending. The soft robot can adjust body stiffness via SMP layers and heating circuit, achieve multiple locomotion modes via the actuator layer, and identify bending curvature through the sensory layer. Actuated by the syringe-pneumatic system, the robot could achieve jumping-gliding locomotion, crawl in two limbs mode. Besides, a microprocessor was attached to the robot's middle part to filter the sensory data then fed the data back to the pneumatic system's controller. The four limbs soft robot can also be reshaped to a four-fingered gripper for picking small items. Meanwhile, soft sensors' data could identify whether an object had been gripped successfully.

Our proposed miniaturized soft robot has several features compared with the previous work [1]–[3]: i) multiple materials are assembled layer by layer to implement a multifunctional miniatured soft robot. ii) the flip-assembling fabrication methods enable multiple high-resolution laser micromachined layers to be assembled rapidly. iii) The embedded mechanosensation enabled the miniatured soft robot to perceive its bending configurations, which would be promising for the robot operating tasks in the unstructured environments.

For future work, we intend to use the miniatured soft robot to investigate soft organisms' body locomotion and analyze the robot's hydrodynamic function under different locomotor patterns, and under different fluid Reynolds number. Scaling down the robots to millimeter-scale for medical applications (Fig. 1(a)). One limitation of the current prototype is that the tethered micro robot motions could be influenced by the tubes and wires. Nevertheless, this limitation may bring in some advantages for future medical applications. For example, the robot will not get lost in the body because of the tether; one can constrain the soft robot from drafting away or even recycle the robot via the tubes or wires. Besides, compared with the untethered microrobot, a tethered robot can continuously perform drug delivery via specific tubes. Implementing a highly integrated, high performance thin, soft robot for medical applications such as robotic surgery and endoscopy would be a promising direction in the future.

ACKNOWLEDGMENT

The authors would like to thank S. Zhuo and S. Wang for helping us implement the experiments.

REFERENCES

[1] W. Hu *et al.*, "Small-scale soft-bodied robot with multimodal locomotion," *Nature*, vol. 554, no. 7690, pp. 81–85, Feb. 2018.
[2] Z. Ren *et al.*, "Multi-functional soft-bodied jellyfish-like swimming," *Nature Commun.*, vol. 10, no. 2703, Jul. 2019, Art. no. 2703.
[3] S. E Chung, X. Dong, and M. Sitti, "Three-dimensional heterogeneous assembly of coded microgels using an untethered mobile microgripper," *Lab. Chip*, vol. 15, no. 7, pp. 1667–1676, Feb. 2015.
[4] H. Ceylan *et al.*, "Mobile microrobots for bioengineering applications," *Lab. Chip*, vol. 17, no. 10, pp. 1705–1724. Apr. 2017.
[5] T. N. Do *et al.*, "Miniature soft electromagnetic actuators for robotic applications," *Adv. Functional Mater.*, vol. 28, no. 18, Mar. 2018, Art. no. 1800244.
[6] M. Sitti, "Miniature devices: Voyage of the microrobots," *Nature*, vol. 458, no. 7242, pp. 1121–1122, Apr. 2009.
[7] B. Mosadegh *et al.*, "Pneumatic networks for soft robotics that actuate rapidly," *Adv. Functional Mater.*, vol. 24, no. 15, pp. 2163–2170, Jan. 2014.
[8] Y. Wang *et al.*, "A biorobotic adhesive disc for underwater hitchhiking inspired by the remora suckerfish," *Sci. Robot.*, vol. 2, no. 10, Sep. 2017, Art. no. 8072.
[9] L. Wen, J. C. Weaver, and G. V. Lauder, "Biomimetic shark skin: Design, fabrication and hydrodynamic function," *J. Exp. Biol.*, vol. 217, no. 10, pp. 1656–1666, May 2014.
[10] L. Wen *et al.*, "Understanding fish linear acceleration using an undulatory biorobotic model with soft fluidic elastomer actuated morphing median fins," *Soft Robot.*, vol. 5, no. 4, pp. 375–388, Aug. 2018.
[11] B. Gorissen *et al.*, "Flexible pneumatic twisting actuators and their application to tilting micromirrors," *Sensors Actuators A: Physical*, vol. 216, no. 1, pp. 426–431, Sep. 2014.
[12] K. C. Bhargava, B. Thompson, and N. Malmstadt, "Discrete elements for 3D microfluidics," *Proc. Nat. Acad. Sci.*, vol. 111, no. 42, pp. 15013–15018, Oct. 2014.
[13] M. Jamal, A. M. Zarafshar, and D. H. Gracias, "Differentially photo-crosslinked polymers enable self-assembling microfluidics," *Nature Commun.*, vol. 2, no. 527, Nov. 2011, Art. no. 527.
[14] G. H. Kwon *et al.*, "Biomimetic soft multifunctional miniature aquabots," *Small*, vol. 4, no. 12, pp. 2148–2153, Dec. 2008.
[15] S. Umrao *et al.*, "MXene artificial muscles based on ionically cross-linked Ti3C2Tx electrode for kinetic soft robotics," *Sci. Robot.*, vol. 4, no. 33, Aug. 2019, Art. no. 7797.
[16] S. Iamsaard *et al.*, "Conversion of light into macroscopic helical motion," *Nature Chemistry*, vol. 6, no. 3, pp. 229–235, Feb. 2014.
[17] T. H. Ware *et al.*, "Voxelated liquid crystal elastomers," *Science*, vol. 347, no. 6225, pp. 982–984, Feb. 2015.
[18] Y., Alapan *et al.*, "Soft erythrocyte-based bacterial microswimmers for cargo delivery," *Sci. Robot.*, vol. 3, no. 17, Apr. 2018, Art. no. 4423.
[19] Y. Kim *et al.*, "Ferromagnetic soft continuum robots," *Sci. Robot.*, vol. 4, no. 33, pp. 7329, Aug. 2019.
[20] M. Garrad *et al.*, "A soft matter computer for soft robots," *Sci. Robot.*, vol. 4, no. 33, Aug. 2019, Art. no. 6060.
[21] V. Cacucciolo *et al.*, "Stretchable pumps for soft machines," *Nature*, vol. 572, pp. 516–519, Aug. 2019.
[22] Y. Hao *et al.*, "A eutectic-alloy-infused soft actuator with sensing, tunable degrees of freedom, and stiffness properties," *J. Micromechanics Microengineering*, vol. 28, no. 2, Jan. 2018, Art. no. 024004.
[23] Y.-L. Park, B.-R. Chen, and R. J. Wood, "Design and fabrication of soft artificial skin using embedded microchannels and liquid conductors," *IEEE Sensors J.*, vol. 12, no. 8, pp. 2711–2718, Dec. 2012.
[24] K. Sim *et al.*, "Metal oxide semiconductor nanomembrane–based soft unnoticeable multifunctional electronics for wearable human-machine interfaces," *Sci. Adv.*, vol. 5, no. 8, Aug. 2019, Art. no. 9653.
[25] R. Guo *et al.*, "Magnetic liquid metal (Fe-EGaIn) based multifunctional electronics for remote self-healing materials, degradable electronics, and thermal transfer printing," *Adv. Sci.*, vol. 6, no. 20, Aug. 2019, Art. no. 1901478.
[26] P. Polygerinos *et al.*, "Modeling of soft fiber-reinforced bending actuators," *IEEE Trans. Robot.*, vol. 31, no. 3, pp. 778–789, May 2015.
[27] N. R. Sinatra *et al.*, "Nanofiber-reinforced soft fluidic micro-actuators," *J. Micromechanics Microengineering*, vol. 28, no. 8, May 2018, Art. no. 084002.
[28] M. J. McHenry and J. Jed, "The ontogenetic scaling of hydrodynamics and swimming performance in jellyfish (*Aurelia aurita*)," *J. Exp. Biol.*, vol. 206, no. 22, pp. 4152–4137, Nov. 2003.
[29] K. J. Quillin, "Kinematic scaling of locomotion by hydrostatic animals: Ontogeny of peristaltic crawling by the earthworm Lumbricus terrestris," *J. Exp. Biol.*, vol. 202, no. 6, pp. 661–674, Mar. 1999.
[30] P. J. Yang, M. Lemons, and D. L. Hu, "Rowing jellyfish contract to maintain neutral buoyancy," *Theor. Appl. Mechanics Lett.*, vol. 8, no. 3, pp. 147–152, May 2018.